

A Comparison between Faraday Tomography and Synchrotron Polarization Gradients

Ka Wai Ho^{1,2}, Ka Ho Yuen², Po Kin Leung¹, and A. Lazarian²

Department of Physics, Chinese University of Hong Kong, Hong Kong

Department of Astronomy, University of Wisconsin-Madison, Madison, USA; kho33@wisc.edu

Received 2019 January 23; revised 2019 October 18; accepted 2019 November 12; published 2019 December 26

Abstract

Observations of synchrotron polarization at multiple frequencies in the presence of Faraday rotation can provide a way to reconstruct the 3D magnetic field distribution. In this paper we compare the well known Faraday Tomography (FT) technique to a new approach, Synchrotron Polarization Gradients (SPGs). We compare the strengths and limitations of the two techniques, and describe their synergy. In particular, we show that in situations when the FT technique fails, e.g., due to insufficient frequency coverage, the SPG can still trace the 3D structure of a magnetic field.

Unified Astronomy Thesaurus concepts: Magnetohydrodynamics (1964); Interstellar medium (847); Interstellar synchrotron emission (856); Interstellar magnetic fields (845); Computational methods (1965)

1. Introduction

Magnetic field structures are very important for key astrophysical processes in interstellar media (ISM) such as the formation of stars (see Mac Low & Klessen 2004; McKee & Ostriker 2007), the propagation and acceleration of cosmic rays (see Jokipii 1966; Yan & Lazarian 2008), the regulation of heat, and mass transfer between different ISM phases (see Draine 2009 for a list of the different ISM phases). Polarized radiation arising from the presence of the magnetic field is also important to explain the enigmatic cosmic microwave background B-modes (Zaldarriaga & Seljak 1997; Caldwell et al. 2017; Kandel et al. 2017).

Synchrotron polarization is widely used to study magnetic fields structure in the sky. However, in the presence of the Faraday rotation it is not trivial to compensate for the distortion from the 2D polarization pattern within the volume-emitting synchrotron radiation. Tracing the actual three-dimensional (3D) magnetic field structure is both a big attraction and an outstanding challenge. Potentially, by combining synchrotron data at different frequencies, one can try to obtain the magnetic field variation along the line of sight (LOS). Burn (1966) first suggested that the Faraday Tomography (FT), i.e., a technique proposed to recover the multi-layer magnetic field structures, can be obtained through a proper Fourier transform from the polarized synchrotron emissions (see Brentjens & de Bruyn 2005, hereafter BB05). A number of works are coming out based on the depolarization of the synchrotron emissions (Robitaille et al. 2017; Dickey et al. 2019; Farnes et al. 2018; Haverkorn 2018; Jelic et al. 2018).

A recently suggested alternative technique of magnetic field tracing employs the Synchrotron Polarization Gradients (SPGs, Lazarian & Yuen 2018b). As discussed in the latter paper, the foundations of the SPGs are routed in the properties of MHD turbulence and turbulent reconnection (Goldreich & Sridhar 1995, Lazarian & Vishniac 1999). As a result, the SPGs trace the local magnetic field through observationally resolved eddies. The applicability of the SPGs to the ISM arises from the fact that ISM is turbulent (Armstrong et al. 1995; Chepurnov & Lazarian 2009, 2010; Burkhart et al. 2015). In the presence of Faraday Rotation, only a certain deepness of the synchrotron emission is effectively collected into the Stokes

parameters. That means the synchrotron polarization map for a specific emitting frequency f corresponds to the plane-of-sky magnetic field variation accumulated up to a certain depth along the LOS. The theory of this effect in the presence of magnetic turbulence is given in Lazarian & Pogosyan (2016). As a result, one can try to obtain the 3D magnetic field structure by utilizing multi-frequency synchrotron emissions. Lazarian & Yuen (2018b) pointed out that by considering the differences of SPGs of polarized synchrotron maps obtained with multi-frequency observations, one can reconstruct the 3D magnetic field structure.

While the two methods for tracing 3D magnetic field both rely on multi-frequency synchrotron emission in the presence of Faraday Rotation, there are significant differences between the foundations of the two methods. This raises a few questions. (1) What are the limitations of the techniques? (2) How precise can the 3D B-field distributions can be traced with these techniques? (3) Are the methods self-consistent? This paper is the first attempt to answer these important questions.

On one hand, the method of SPGs relies on the fact that turbulence is ubiquitous while the FT provides self-consistent 3D mapping of the underlying regular magnetic field. On the other hand, the method of FT has a much higher requirement on the number of frequencies compared to the SPG (e.g., Li et al. 2011). In addition, the LOS magnetic field strength information³ is not available for the FT but is possible to obtain using SPG (see Lazarian & Yuen 2018b).

We would therefore like to compare the two techniques in this paper through numerical simulations of the uniform and isothermal turbulent medium. Instead of confronting the techniques we search for their synergy. In what follows, we briefly describe the numerical code and setup for simulations in Section 2, the methodology related to FT and SPGs in Section 3, and the performance of the two methods in Sections 4 and 5. A discussion and exploration of the the synergy of the two methods

³ While the Faraday Measure is proportional to the product of cumulative thermal electron density and LOS magnetic field strength, RM $\propto \int dz n_{e,th} B_z$, it is impossible to obtain the true magnetic field strength along the LOS due to two reasons. (1) The thermal electron distribution along the LOS is not given and (2) the contribution of magnetic field strength to the RM would be canceled out in the case of a sufficient field reversal along LOS. See Lazarian & Pogosyan (2016) for more details.

Table 1
Simulations Used in Our Current Work

Model	$M_{ m s}$	$M_{ m A}$	$\beta = 2\left(\frac{M_{\rm A}}{M_s}\right)^2$
Ms0.2Ma0.02	0.2	0.02	0.02
Ms0.4Ma0.04	0.4	0.04	0.02
Ms0.8Ma0.08	0.8	0.08	0.02
Ms1.6Ma0.16	1.6	0.16	0.02
Ms3.2Ma0.32	3.2	0.32	0.02
Ms6.4Ma0.64	6.4	0.64	0.02
Ms0.2Ma0.07	0.2	0.07	0.22
Ms0.4Ma0.13	0.4	0.13	0.22
Ms0.8Ma0.26	0.8	0.26	0.22
Ms1.6Ma0.53	1.6	0.53	0.22
Ms0.2Ma0.2	0.2	0.2	2
Ms0.4Ma0.4	0.4	0.4	2
Ms0.8Ma0.8	0.8	0.8	2
Ms0.13Ma0.4	0.13	0.4	18
Ms0.20Ma0.66	0.20	0.66	18
Ms0.26Ma0.8	0.26	0.8	18
Ms0.04Ma0.4	0.04	0.4	200
Ms0.08Ma0.8	0.08	0.8	200
Ms0.2Ma2.0	0.2	2.0	200

Note. The magnetic criticality $\Phi = 2\pi G^{1/2} \rho L/B$ is set as 2 for all simulation data. Their resolution is 480^3 .

takes places in in Sections 6 and 7, and a summary is provided in Section 8.

2. Numerical Simulations

Simulation setup. The numerical 3D MHD simulations were used in Lazarian & Yuen (2018a, 2018b) by setting up a 3D, uniform, isothermal turbulent medium. We use a range of Alfvénic Mach number $M_{\rm A}=V_L/V_{\rm A}$ and sonic Mach number $M_{\rm S}=V_L/V_{\rm S}$, where V_L is the injection velocity; and $V_{\rm A}$ and $V_{\rm S}$ are the Alfvén and sonic velocities, respectively. The numerical parameters are listed in Table 1 in sequence of ascending values of media magnetization $\beta=2(M_{\rm A}/M_{\rm S})^2$.

Synthesis of position–position-frequency (PPF) cubes. We synthesize the PPF cubes following the procedures in Lazarian & Yuen (2018b), which we summarize as below. To characterize the fluctuations of the synchrotron polarization, one can use different combinations of the Stokes parameters (see Lazarian & Pogosyan 2012). In this paper, we follow the approach in Lazarian & Pogosyan (2016) and focus on the measure of the linear polarization P, which is

$$P = Q + iU, (1)$$

where Q and U are the Stokes parameters.

We consider an extended synchrotron region, where both synchrotron emission and Faraday rotation are taking place simultaneously. Special cases, e.g., where the regions of synchrotron radiation are separated from those of Faraday rotation (see the analytical description in Lazarian & Pogosyan 2016), can be analyzed easily following the same treatment presented below. The polarization of the synchrotron emission at the source is characterized by the polarized intensity density $P_i(X, z)$, where X is the two-dimensional plane-of-sky vector and z is the distance along the LOS. The polarized intensity detected by an observer in the direction X at the wavelength λ is

given by

$$P_i(X, \lambda^2) = \int_0^L dz P_i(X, z) e^{2i\lambda^2 \Phi(X, z)}.$$
 (2)

The region is extended up to the scale L and the Faraday rotation measure (RM) Φ (z) is given by (see BB05)

$$\Phi(z) \propto \int_0^z n_e(z') B_z(z') dz' \tag{3}$$

where B_z is the strength of the LOS component of the magnetic field and z is the distance.

We use the definition of synchrotron polarization in Lazarian & Pogosyan (2016), thus ignoring the wavelength dependences of synchrotron polarization arising from the cosmic ray spectrum. This means the polarization source term $P\left(X,z\right)$ will be wavelength-independent, while the observed polarization will be wavelength-dependent due to Faraday rotation only. Similar to Lazarian & Yuen (2018b), we assume the cosmic-ray index $\gamma=2$ since Lazarian & Pogosyan (2012) showed the marginal effect of γ on the spatial variations in the Stokes parameters. That means we can express the Stokes Q and U as

$$Q(X, z) \propto pn_e(B_x^2(z) - B_y^2(z))$$

$$U(X, z) \propto pn_e 2B_x(z)B_y(z),$$
(4)

where X is the two-dimensional plane-of-sky vector, p is the polarization fraction, which is assumed to be constant, B_r , B_v are the two directions of the plane-of-sky magnetic field, and n_e is the density of relativistic electrons. The definitions of the Stokes parameters above correspond to the synchrotron intensity at the source $I(X, z) \propto B_x^2(z) + B_y^2(z)$. In our investigation, we cover the frequency range between 3×10^7 and 3×10^{11} Hz. With regard to spectral resolution, since the frequency selection rule is different for two methods (see Section 3.3 for detailed discussion), the spectral resolution is not fixed but dynamical with respect to the wavelength. For SPG, we performed 20 synthetic observations of different frequencies, with equal spacing in frequency square space within the frequency range. For FT, we performed 500 synthetic observations of different frequency with equal spacing in wavelength square space within the wavelength range, which could resolve the Faraday dispersion function $F(\phi)$ in a high resolution. Therefore, the resolving power can reach up to $||\phi_{\rm max}|| \approx 17 \ {\rm rad \ m^{-2}}, \ \delta\phi \approx 0.034 \ {\rm rad \ m^{-2}}, \ {\rm and}$ $\phi_{\rm max-scale} \approx 3\,\times\,10^6\,{\rm rad~m^{-2}}.$

3. FT and SPGs

3.1. Faraday Tomography

The concept of FT was first suggested by Burn (1966). The method utilizes the fact that the Faraday rotation integral of synchrotron polarization along the LOS is effectively a Fourier transform of the complex polarized brightness per unit Faraday depth $F(\phi)$:

$$P(\lambda^2) = Q + iU = \int_{-\infty}^{\infty} F(\phi) e^{2i\phi\lambda^2} d\phi, \tag{5}$$

where λ is the observed wavelength, $P(\lambda^2)$ is the complex polarized surface brightness in terms of Stoke parameters Q and U, and $\phi \propto \int dz n_{\rm th} B_z$ is the Faraday depth, with $n_{\rm th}$ being

the number density of the thermal electrons and B_z is the LOS component of the magnetic field. Performing the inverse Fourier transform, one can easily acquire $F(\phi)$:

$$F(\phi) = \int_{-\infty}^{\infty} P(\lambda^2) e^{-2i\phi\lambda^2} d\lambda^2$$
 (6)

which provides the 3D Magnetic field information as a function of ϕ . Since λ^2 only lies in the positive real space, the inverse Fourier transform cannot be computed accurately unless the negative part of λ^2 is provided. BB05 provided a solution to the problem by introducing the window function $W(\lambda^2)$ to reconstruct $F(\phi)$. The window function is non-zero in the range of observed λ^2 and is otherwise zero. BB05 then defined the observed polarized surface brightness as

$$\tilde{P}(\lambda^2) = P(\lambda^2) W(\lambda^2), \tag{7}$$

As a result, the complex polarized brightness that includes the window $\tilde{F}(\phi)$ can be written as

$$\tilde{F}(\phi) = F(\phi) * R(\phi) = K \int_{-\infty}^{\infty} \tilde{P}(\lambda^2) e^{-2i\phi(\lambda^2 - \lambda_0^2)} d\lambda^2, \quad (8)$$

where $R(\phi)$ is the rotation measure transfer function (RMTF; see BB05):

$$R(\phi) = \frac{\int_{-\infty}^{\infty} W(\lambda^2) e^{-2i\phi(\lambda^2 - \lambda_0^2)} d\lambda^2}{\int_{-\infty}^{\infty} W(\lambda^2) d\lambda^2}.$$
 (9)

The function K is

$$K = \left(\int_{-\infty}^{\infty} W(\lambda^2) d\lambda^2\right)^{-1},\tag{10}$$

and a parameter λ_0 is introduced to Equations (8) and (9) in order to improve the the behavior of RMTF. The optimal λ_0^2 is the mean of λ^2 sample values obtained by the telescope. However, the term λ_0 would cause a further rotation effect, which is similar to the Faraday rotation when tracing the plane-of-sky magnetic field directions along the LOS using FT. So, we would remove the term in this paper. (See Section 4.1.3 for further discussions).

The technique introduced by BB05 is referred to as RM synthesis. It shows promise for obtaining the 3D tomography magnetic field structure. The requirement for the technique to work is to have enough synchrotron polarization measurements at different frequencies.

To calculate $F(\phi)$ in numerical simulations, we consider a column of data along the LOS in a 3D MHD numerical data cube and divide this column into n segments. Each segment contains density, magnetic field (such as Q and U), and rotation measurement ϕ information. In this setting the polarization can be calculated as, according to BB05, as

$$P(\lambda^2) = \sum_{k=1}^{n} P_k e^{-2i\phi_k \lambda^2},\tag{11}$$

where $P_k = Q_k + iU_k$, representing the P_k at different ϕ_k . The Faraday dispersion function can then be expressed as

$$F(\phi) = \sum_{k=1}^{n} \int_{-\infty}^{\infty} P_k e^{-2i\phi_k \lambda^2} e^{-2i\phi \lambda^2} d\lambda^2.$$
 (12)

Although we cannot determine $P(\lambda^2)$ when $\lambda^2 < 0$, it is still useful to assume Equation (12) holds by assuming

 $P(\lambda^2 < 0) = 0$:

$$F(\phi) \approx \sum_{k=1}^{n} P_k \delta(\phi - \phi_k), \tag{13}$$

which suggests that $|F(\phi)|$ can be decomposed into n delta functions $\delta(\phi - \phi_k)$, peaked at ϕ_k . Note that Equation (13) and the reconstructed Faraday dispersion function $\tilde{F}(\phi)$ are not equivalent but share many similarities.

3.2. Synchrotron Polarization Gradient

Effective measurable distance due to the Faraday screening effect. In Lazarian & Pogosyan (2016) and Lazarian & Yuen (2018b) the effective measurable distance $L_{\rm eff}$ arising from Faraday depolarization is introduced, and refers to the LOS distance over which the Faraday rotation phase of the synchrotron emission source is less than unity. Mathematically,

$$\frac{L_{\rm eff}}{L} \sim \frac{1}{\lambda^2 L} \frac{1}{\phi} \tag{14}$$

where L is the cloud thickness. Synchrotron polarization from distances larger than $L_{\rm eff}$ manifests as noise in the resultant Stokes maps (see Lazarian & Yuen 2018b). In contrast to measuring FT, which depends on the profile of $B_{\rm LOS}$ and its variations to ϕ , $L_{\rm eff}$ in SPG would provide a more robust measure that does not depend on the sign on $B_{\rm LOS}$. As shown in Lazarian & Pogosyan (2016), the measure can be introduced for the random magnetic field. It preserves the relation between the depth and measured parameters, while FT requires extra information about the density and magnetic field along the LOS.

Block averaging for gradient calculations. Gradients of polarization are calculated by taking the values of polarization in the neighboring points and dividing them over the distances between the points following the recipe of Yuen & Lazarian (2017). In this work, we focus on the smallest-scale contribution, as we did in Lazarian & Yuen (2018a, 2018b), which provides the criteria for the gradients to be perpendicular to the magnetic field by investigating the indexes of the power spectrum and correlation function anisotropy. As we are using the same set of simulations used in Lazarian & Yuen (2018b), the criteria in Lazarian & Yuen (2018b) are automatically satisfied.

3.3. Frequency Sampling between the SPG and FT

As we discussed in Section 2, there is a crucial difference in choosing the width of the frequency band for the two techniques.

In the case of FT, since we are performing a Fourier transform with the term $e^{2i\phi\lambda^2}$ in λ^2 space, the dependencies of the frequency width in FT are related to $\delta\lambda^2$ but $\delta\frac{1}{\lambda^2}$ for SPG. Additionally, they also have different meanings when changing the frequency width. For FT, BB05 brings out the following relation between ϕ and $\delta\lambda^2$ as

$$||\phi_{\text{max}}|| \approx \frac{\sqrt{3}}{\delta \lambda^2}.$$
 (15)

The $\delta \lambda^2$ term controls the maximum ϕ that is not affected by the $m\pi$ ambiguities problem. To maximize the usable range of ϕ , the robust approach is to narrow the frequency width.

Sometimes it is necessary for the observer to narrow the width of the synchrotron emission along which the LOS is lined on a large $|\phi|$. Therefore, the FT requires more data points to retain its accuracy.

For the SPG technique, we can get the relation from Equation (14) and bring out the result

$$\delta L_{\rm eff} \propto \delta \frac{1}{\lambda^2}.$$
 (16)

The width of the frequency band controls how thick the layer is along the LOS. Increasing the number of data points within the frequency band can provide a more detailed morphology within the region. One of the advantages of this method is that the result will not be affected by the $m\pi$ ambiguities problem. Observers have the flexibility to choose the frequency bandwidth.

3.4. Testing Method

Alignment measure (AM). To quantify how good two vector fields are aligned, we employ the AM that is introduced in analogy with the grain alignment studies (see Lazarian 2007):

$$AM = 2\langle \cos^2 \theta_r \rangle - 1, \tag{17}$$

(see González-Casanova & Lazarian 2017; Yuen & Lazarian 2017) with a range of [-1, 1] measuring the relative alignment between the 90°-rotated gradients and magnetic fields, where θ_r is the relative angle between the two vectors. A perfect alignment gives AM = 1, whereas random orientations generate AM = 0. In what follows we use AM to quantify the alignments of polarization gradients in respect to magnetic field.

4. Results

4.1. FT

4.1.1. The Reconstructed Faraday Dispersion Function of ISM

To use the Faraday tomography method, we use the reconstructed Faraday dispersion function $\tilde{F}(\phi)$ instead of the Faraday dispersion function $F(\phi)$ because (i) as explained above, it is only possible to obtain $\tilde{F}(\phi)$ from observational data, (ii) both functions share similar spiky features with respect to the Faraday RM, and (iii) the corresponding ϕ -values of those peaks are similar for both functions. To demonstrate the points, Figure 1 shows $\tilde{F}(\phi)$ from a simulation sample and compare with $F(\phi)$. They match the properties that Equation (13) describes. The function $\tilde{F}(\phi)$ still contains the spiky feature we observed in $F(\phi)$. Moreover, the positions of the spikes in $\tilde{F}(\phi)$ are consistent to those in $F(\phi)$. Therefore, we can use Equation (13) and describe the features we calculated using the $\tilde{F}(\phi)$.

The reconstruction of the Faraday dispersion function in simulations is rather trivial since the number of segments n in Equation (13) corresponds to the number of frequency measurements in observations. It should be possible to obtain the magnetic field distributions exactly, provided that one has sufficiently large n in Equation (13). However, increasing the number of measurements is very costly, as the Nyquist condition for the reconstruction of Faraday dispersion function grows with the square root of n; that means to increase the signal-to-noise by a factor of 2 one has to increase the number of measurements four times.

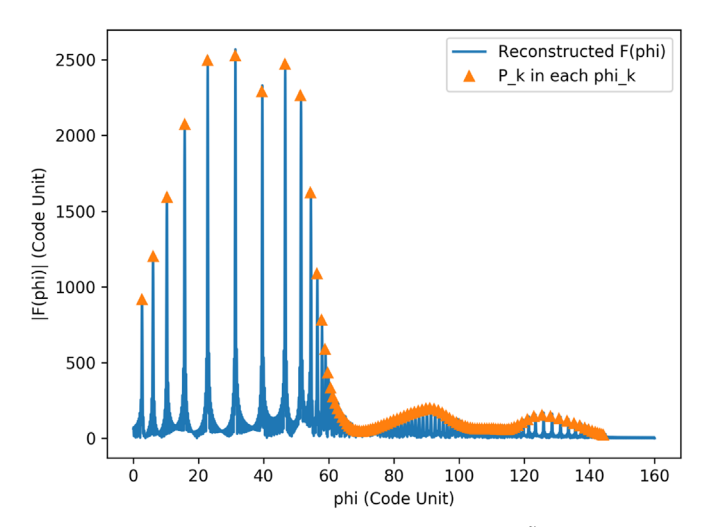


Figure 1. Comparison plot of between the actual P_k and \tilde{F} . The samples are randomly chosen from a column of pixels along the line of sight in a 3D MHD simulation Ms3 2Ma0 32.

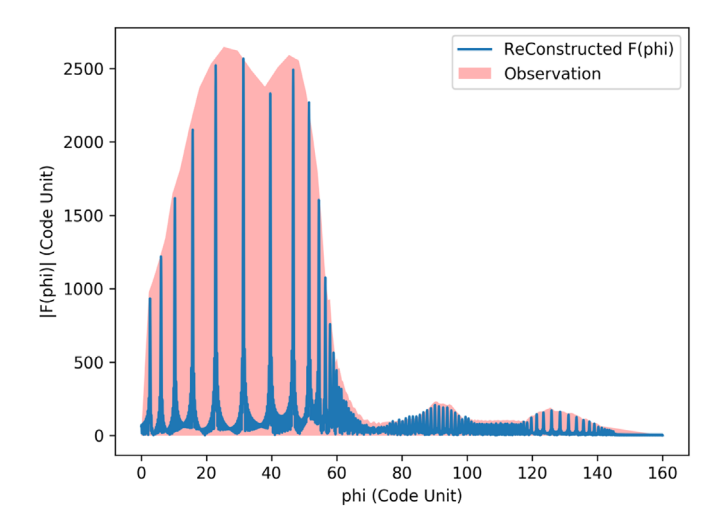


Figure 2. Illustration of the difference between simulation data and observation.

In Figure 1 we observed a lot of δ -like structures sparsely spaced across ϕ . The spaces between the δ -like structures are referred to as gaps, while the δ -like structures themselves are referred to as peaks. However, we do not expect to see any peaks in observation due to observational constraints such as the limited resolving power. The pink shaded area of Figure 2 shows what would be seen in observations if the FT were distributed as in Figure 1. While in simulations the reconstructed $F(\phi)$ along ϕ are segmented, the observed $F(\phi)$ is continuous with respect to $F(\phi)$. It is still possible to resolve the peaks from the observed $F(\phi)$ through mapping the peaks of the observed $F(\phi)$ as shown in Figure 2, provided that the resolution of the instrument is high enough.

4.1.2. Determining the Magnetic Field Orientation Using FT

The advantage of the FT over other methods is the high precision of determining the plane-of-sky component of the magnetic field as long as there are enough frequency channels that satisfy the Nyquist criterion. With a correct selection of frequency band in observation, one can determine the peaks in the Faraday dispersion function without difficulties. We would

Table 2

Accuracy of the FT Method for Different Frequency Bands and LOS B-fields

LOS B-field type:	Ordered	Chaotic	Chaotic
Frequency (Hz):	$3 \times 10^8 - 3 \times 10^{11}$	$3 \times 10^8 - 3 \times 10^{11}$	$3 \times 10^7 - 3 \times 10^{11}$
Model	AM	AM	AM
Ms0.4Ma0.04	0.92	0.24	0.70
Ms0.8Ma0.08	0.90	0.26	0.81
Ms1.6Ma0.16	0.88	0.28	0.81
Ms3.2Ma0.32	0.87	0.26	0.74
Ms6.4Ma0.64	0.86	0.23	0.60
Ms0.4Ma0.32	0.82	0.99	0.27
Ms0.8Ma0.264	0.81	0.95	0.28
Ms1.6Ma0.528	0.76	0.70	0.23
Ms0.4Ma0.4	0.83	0.95	0.87
Ms0.8,Ma0.8	0.65	0.73	0.40
Ms0.132Ma0.4	0.78	0.94	0.94
Ms0.264Ma0.8	0.63	0.55	0.73
Ms0.04,Ma0.4	0.74	0.92	0.94
Ms0.08,Ma0.8	0.75	0.72	0.64

Note. The bold font is used to emphasize the values of AM corresponding to high alignment.

like to illustrate the power of FT using the numerical simulations listed in Table 1.

Table 2 shows the AM of the FT reconstructed plane-of-sky component magnetic field compared to the true magnetic field in numerical simulations. To get these results, we first convert the numerical cube to a PPF cube using the approach in Section 2 and then we compute the \tilde{F} . After that, we locate the most significant three peaks for which the real and imaginary parts represent the Stokes parameters Q and U. The three peaks we located in ϕ space are converted to the magnetic field measurements that we compare with the real magnetic field using the AM (see Section 2). When we are computing the AM we randomly select 300 columns. We also use the ϕ value found from those three peaks and compare to the exact values of the polarization angle available from the simulations. Finally, we compare both angles and get the AM values for each of them. There are subtle differences between the cases whether the mean field or the turbulent field dominates along the LOS (Lazarian & Pogosyan 2016) and careful studies have to be done these cases. To test this, we perform tests in both cases with ordered and chaotic LOS B-fields. For the ordered B-field case, we rotate the simulation cube such that the mean field direction is pointing to the observer. For the chaotic field case, we further rotate the cube so that the mean field direction is parallel to the plane-of-sky. One can see that for both cases of ordered and chaotic LOS B-fields the AM is pretty high, with an average value of $\sim 0.7-0.8$, if we pick the correct frequency band.

4.1.3. The Improvement of FT and Its Impact

Note that we do not apply the technique involving a multiplicative factor of $e^{2i\phi\lambda_0^2}$ in the calculation of \tilde{F} as suggested

in BB05. BB05 thought that this factor could influence the phase rotation of \tilde{F} in both real and imaginary space, thus affecting the tracing power of FT. However, we have shown that FT performs well even without this factor. Also, with the extra factor, Equation (18) will become

$$F(\phi) = \sum_{k=1}^{n} \int_{-\infty}^{\infty} P_k e^{-2i\phi_k \lambda^2} e^{-2i\phi(\lambda^2 - \lambda_0^2)} d\lambda^2$$

$$\approx \sum_{k=1}^{n} P_k e^{2i\phi_k \lambda_0^2} \delta(\phi - \phi_k)$$
(18)

Compared to Equations (13), (18) contains an extra term $e^{2i\phi_k\lambda_0^2}$. This term will not affect the features of $|F(\phi)|$ at ϕ space since $e^{2i\phi_k\lambda_0^2}$ will be canceled during the calculation by its conjugate term. So, the peak value and the location of the δ function will not be changed. However, if we use the same treatment as we did on $|F(\phi)|$ for Q_k and U_k , then the extra term $e^{2i\phi_k\lambda_0^2}$ will not be canceled but induce extra Faraday rotation. In fact, there is a similar mathematical origin for the expressions from Faraday rotation $e^{-2i\phi_k\lambda_0^2}$ and the term in Equation (18) that is $e^{2i\phi_k\lambda_0^2}$. As a result, the inclusion of the $e^{2i\phi_k\lambda_0^2}$ term will introduce an additional rotation of $-\phi_k\lambda_0^2$ degree for the polarization angle ϕ_k . The removal of the $e^{2i\phi_k\lambda_0^2}$ term would make the polarization angle more physically justified.

4.2. The Performance of SPG in Tracing the 3D Magnetic Field

To compare the performance of the SPG tomography proposed in Lazarian & Yuen (2018b) with the FT, we divide the axis along the LOS into 20 slices, which corresponds to $L_{\rm eff}/L$ from 0.05 to 1.0 with a separation of 0.05. This allows us to trace the 2D magnetic field structure at different depths. The frequencies required are computed from Equation (14).

After a correct selection of frequency bands, which corresponds to a set of effective LOS thicknesses, we can then get the synchrotron polarization derivative map from calculating

The whole process for FT is expensive, since a two-step process is required to convert the simulation cubes to the Faraday dispersion function, namely from the position–position–position (PPP) cubes to the PPF cubes and finally to PP ϕ cubes. Both processes have the computational complexity of $O(N^3 \times N_f)$ and $O(N^3 \times N_\phi)$, where N, N_f , and N_ϕ are the resolutions of simulations, number of frequency bands, and number of RM channels, respectively. We assume the $N_f = N_\phi$ in this study. Apart from that, computing AM also requires the computational complexity of $O(N^3 \times N_\phi)$ to trace back the local maximum. So, checking pixels randomly provides a more efficient approach in checking the accuracy of FT.

Table 3

Accuracy of the SPG Method in Different LOS B-fields, (Columns without AM Values Correspond to the Case in which the Required Frequency to Calculate the SPG is Less then 10⁷ MHz)

LOS B-field Type: Model	Ordered AM	Chaotic AM
Ms0.4Ma0.04	0.21	0.50
Ms0.8Ma0.08	0.25	0.63
Ms1.6Ma0.16	0.39	0.70
Ms3.2Ma0.32	0.23	0.68
Ms6.4Ma0.64	0.25	0.50
Ms0.4Ma0.32	0.17	/
Ms0.8Ma0.264	0.19	0.48
Ms1.6Ma0.528	0.26	0.50
Ms0.4Ma0.4	/	/
Ms0.8Ma0.8	,	,
Ms0.132Ma0.4	,	,
Ms0.264Ma0.8	,	,
Ms0.04Ma0.4	,	,
Ms0.08Ma0.8	/	/

the difference of polarized intensity $\bar{\Phi} = \sqrt{\Delta Q^2 + \Delta U^2}$ by

$$\Delta Q = Q(f_{i+1}) - Q(f_i),$$

 $\Delta U = U(f_{i+1}) - U(f_i),$ (19)

where f_{i+1} and f_i are two neighboring frequencies. The two maps contain information on the cumulative magnetic morphology in the corresponding depth and computing the differences of gradient orientation can determine the 3D magnetic morphology between the two LOS depths $\delta L_{\rm eff} = L_{\rm eff}(f_{i+1}) - L_{\rm eff}(f_i)$. We use the block averaging technique (see YL17) to obtain the statistical measurement of gradient orientation within a sampling region. In our calculations we choose the block size to be 30×30 pixels. Table 3 shows the AM from different numerical cubes following our treatment.

A clear trend shown in the table is that SPG traces the magnetic morphology with higher accuracy compared to that for the chaotic LOS field. This follows from the differences in the localization of L_{eff} for the cases of regular and chaotic fields (Lazarian & Pogosyan 2016). For the ordered LOS magnetic field case we get the AM around 0.2-0.3, which agrees well with the results in Lazarian & Yuen (2018b). All gradient techniques share the same foundation of anisotropic MHD turbulence, i.e., the turbulent eddies are elongated along the local magnetic field directions described in Goldreich & Sridhar (1995) and Lazarian & Vishniac (1999). The anisotropy properties will affect the structure of other observables, e.g., integrated intensities, velocity centroids, velocity channels, and also synchrotron intensities. How the gradient techniques perform is highly related to whether or not the environment is dominated by turbulence, and how anisotropic the system is. In our case of an ordered B-field, the mean magnetic field direction is pointing along the LOS. Since the turbulent eddies are all aligned to the local field and most of our numerical cubes have strong magnetization, when observing along the mean field only weak or even no anisotropy can be detected. This also explains why the model with lower M_A traces magnetic fields better.

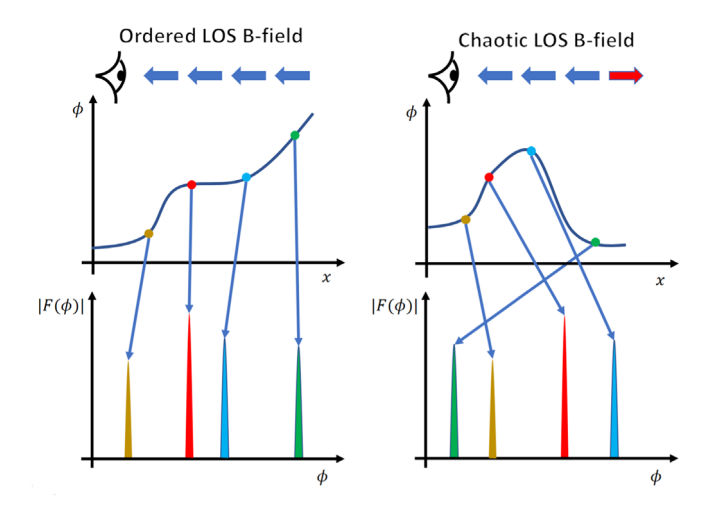


Figure 3. Illustration of two types of LOS B-field and how they affect the order of the δ function.

5. What Technique(s) Should We Select?

5.1. LOS Information along the ϕ Axis

In order to understand the magnetic field from different depths of $\tilde{F}(\phi)$, we should first understand the relation between the δ functions at ϕ and LOS axes. On the scale of the resolution, the correct identification of the position of δ function is closely related to how ordered the LOS B-field is. Depending on the strength of the mean and fluctuating magnetic fields, we can classify the magnetic field conditions into two cases. If the LOS B-field is highly ordered, e.g., when the B-field direction is pointing either toward or away from the LOS observer, each ϕ_k is unique and we can relate the order in the location of the δ function in the reconstructed distribution and the order in the location of emitters in the source. If the LOS B-field is chaotic, i.e., it points both toward and away from the observer, this relation fails. Figure 3 illustrates both cases. In a magnetized environment, the LOS magnetic field structure is usually determined by the orientation of the mean field with respect to the observer. For the SPGs, problems arise when the mean field is directed exactly toward or away form the observer. To solve the problem of a complicated dependence of ϕ on the LOS, a physical model of the local interstellar medium should be built up to relate the two physical quantities (Jelic et al. 2015; Van Eck et al. 2017). However, such a model requires additional measurements.

5.2. Synergy of SPGs and FT

SPGs are a very new tool, therefore the corresponding procedures of restoring the 3D structure require refinement and improvements. We expect that the AM in Table 3 will improve as the technique matures. Nevertheless, even at this point we can clearly see the synergy between the SPGs and the FT.

As we showed in Section 4.1.1, the LOS B-field structure is critical for determining the positions of synchrotron emission sources in the $\tilde{F}(\phi)$. Since the LOS B-field is turbulent in the ISM, tracing 3D B-field structure with FT is difficult in many cases, especially if the mean field is close to perpendicular to the LOS. This is exactly the case, however, when the SPGs can be most useful. As we discussed above, the SPGs have trouble tracing magnetic field structure when the mean field is nearly

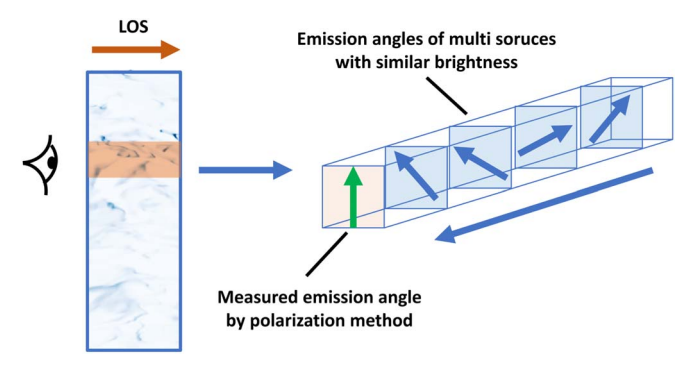


Figure 4. Illustration of how multiple emission sources with similar intensity changes the results of the emission angle measurement.

parallel to the LOS. At the same time, SPG performs best when the mean magnetic field is perpendicular to the LOS.

The traditional polarization method used widely in the astronomical community provides one polarization angle vector per pixel. It is usually interpreted as the 2D B-field direction at that pixel. However, the polarization direction that we measured is actually a sum of the Stokes parameters of that column and the direction of polarization is affected by the Faraday rotation (see Equation (11)). While the Faraday rotation effect can be minimized by observing the polarization at high frequencies, even in this case the angle that we measure is a mean angle of synchrotron emission from multiple synchrotron sources along the LOS. If the LOS emission is dominated by one bright emission source, the measured polarization angle is close to the polarization angle at the source. In an extreme case where we have multiple sources with comparable brightness, the measured polarization angle may be misleading. As a simple example, consider two synchrotron polarization sources of similar brightness having 0 and $\frac{\pi}{4}$ polarization angles, which are illustrated by Figure 4. The angle measured in this case is $\sim \frac{\pi}{8}$ and this fails to represent the underlying magnetic field information for either of the sources. Multiple bright sources along the LOS is very common. Unfortunately, it is impossible to tell how many sources are along the LOS, and their respective weights, by simply increasing the observing frequency.

On the contrary, the FT method (Burn 1966, BB05) has the ability to detect the number of emission sources along the LOS. The amplitude of $\delta(\phi)$ functions at the Faraday dispersion function represents the brightness of each source. By counting the number of peaks of the Faraday dispersion function, not only do we know the number of intensive sources along the LOS, but also the 2D magnetic field structure within the source.

The mathematical nature of the FT method allows resolution of the magnetic field structure with respect to the LOS distance from synchrotron emissions with different frequencies. We can even know the intensity distribution along the LOS from this method. It also gives a high AM that allows us to trace the magnetic field orientation in whatever direction the mean magnetic field points to. However, we lose the positional information during the move from λ^2 space to ϕ space. Due to the nature of the Faraday rotation, the magnetic field information stored in a certain ϕ_i but in different positions $F(X_i, \phi_i)$ and $F(X_j, \phi_i)$ could represent the different depths along the LOS. In order to construct the 3D POS magnetic field morphology of the FT method, we require extra information on the magnetic field and density profile along the LOS.

On the other hand, SPG depicts the magnetic field structure quite well. It can map the 2D magnetic morphology at different depths and even the 3D structure shown in Lazarian & Yuen (2018b). Unlike FT, which is applied to all the environments, this method comes with requirements for the environment. In theory, the method of SPG requires the system to have anisotropic turbulence satisfying the spectral conditions suggested by Lazarian & Yuen (2018b), namely the spectral slope has to be steeper than -1 and the local anisotropy has to be along the local magnetic field direction. In fact, the electron spectrum studies from Armstrong et al. (1995), later extended by Chepurnov & Lazarian (2010), showed that the turbulence spectrum is -5/3 for 15 orders of magnitudes, including the scale where synchrotron emissions are significant. Moreover, the anisotropy of the statistical measures available through observations is a well established fact proven with both synthetic observations and actual observational data (see Lazarian et al. 2002; Esquivel & Lazarian 2005; Heyer et al. 2008; Yuen et al. 2018).

Although both techniques advertise that they can provide magnetic field information tomographically, their products are different and it is difficult to directly compare them. For instance, one can identify the bright sources using FT while constructing the 3D field morphology using SPG. The information acquired by both methods is complementary but a side-by-side comparison requires further conversion between the two methods.

6. Discussion

6.1. Requirements for the Instruments

It has been shown in Section 5.2 that SPG and FT techniques are actually complementary. The SPG method requires far less data points compared to FT, and it can be used to scan though the whole region. The method can then provide a 2D magnetic field structure of the whole environment with good accuracy (AM 0.6–0.7). Apart from tracing the direction of the magnetic field, the SPG can be used to test the magnetization information. The corresponding technique of obtaining a distribution of Alfvénic Mach numbers $M_{\rm A}$ was demonstrated in Lazarian & Yuen (2018a).

The FT technique (Burn 1966, BB05, see also Farnes et al. 2018; Haverkorn 2018; Jelic et al. 2018; Dickey et al. 2019) provides a high-accuracy restoration of the magnetic field (AM 0.8–0.9) in the case when the Faraday depth is a straightforward and monotonic function of distance. However, it requires more frequency measurements to maintain high resolution. In BB05, the resolution of the Faraday dispersion function is calculated as

$$\delta\phi = \frac{2\sqrt{3}}{\Delta\lambda^2}.\tag{20}$$

⁵ The anisotropy of MHD turbulence has been has been known for a while (see Higdon 1984). It is also a part of Goldreich & Sridhar's (1995) picture. It is essential for the SPGs, however, that the anisotropy is present not in terms of mean magnetic field, but in terms of local magnetic field, i.e., the magnetic field at the location of turbulent eddies. This concept is not a part of the original Goldreich & Sridhar (1995) model, but it was introduced in later publications. It follows from turbulent reconnection theory (Lazarian & Vishniac 1999) and is supported by numerical simulations by Cho & Vishniac (2000), Maron & Goldreich (2001), and Cho et al. (2002).

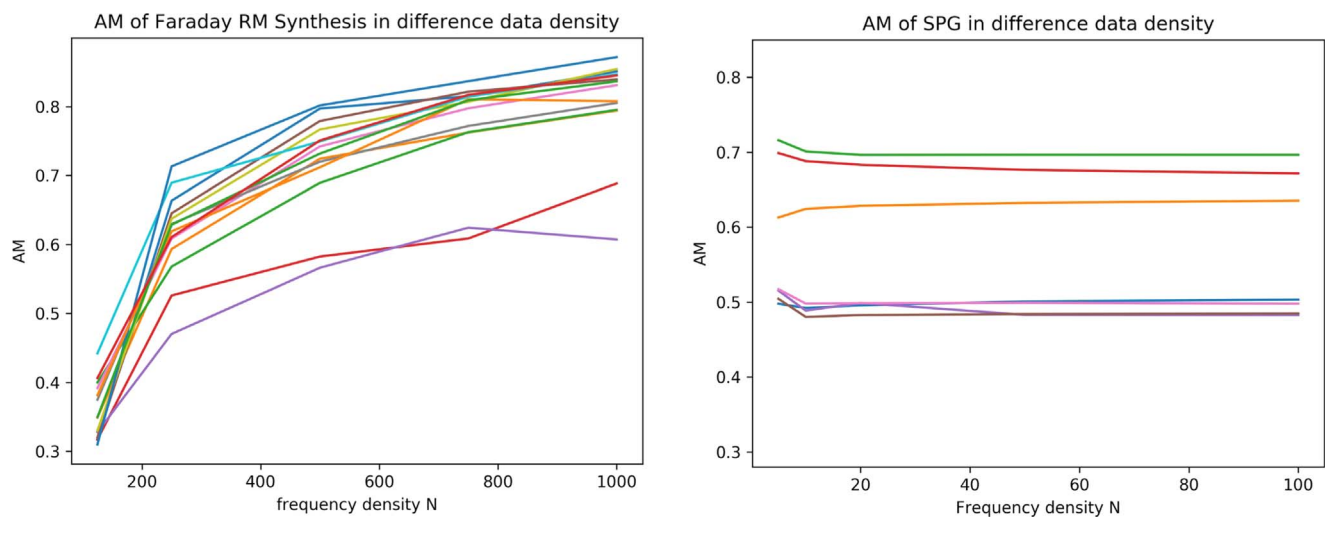


Figure 5. Plot of the AM (y-axis) and frequency density (x-axis) in different numerical simulations listed in Section 2. Every color line represents a numerical simulation. The left panel is the FT plots and the right panel is the SPG plots.

The resolution of the Faraday dispersion function is very sensitive to the frequency density upon combining Equations (15) and (20):

$$\frac{\delta\phi}{\phi_{\text{max}}} = \frac{2\delta\lambda^2}{\Delta\lambda^2} = \frac{2}{N}.$$
 (21)

Here $N=\Delta\lambda^2/\delta\lambda^2$ is the frequency density in a certain frequency band for FT (the definition would change to $N=\Delta f^2/\delta f^2$ for SPG), meaning the total number of N measurements observed in a particular frequency band $\Delta\lambda^2$ with frequency width $\delta\lambda^2$. The resolution then affects the accuracy of the FT technique probing the direction of the magnetic field. To test how the frequency density affects the accuracy, we perform a test for both techniques with different frequency densities in Figure 5.

There is a clear trend in which the accuracy of the FT technique drops with respect to the frequency density in all of our simulations. For instance, when the frequency density drops to 250, the accuracy of the FT drops to the range of 0.5–0.7. Note that the SPG technique can achieve the same accuracy with only 20 frequency points. The performance of FT becomes worse when one further decreases the frequency density to 125 frequency points. On the other hand, SPG provides a very stable result, with only small fluctuations even for very low-frequency density measurements like 5 and 10 frequency points.

Also note that FT is sensitive to the frequency range covered by the instrument when tracing emission with different physical conditions. As shown in this paper and previous literature, changing the observational frequency range can improve the performance for emission with different types of LOS B-fields (see Table 2) and trace the emission region with different typical distances along the LOS (see Dickey et al. 2019).

We demonstrated in Section 4.2 that SPG is flexible when applied to data with different frequency resolutions and it can plausibly construct 3D magnetic field morphology with high precision. To better resolve the Faraday depth structure, FT requires high-precision instruments like the Low-Frequency Array. Therefore, outlining the synergy between SPG and FT can be beneficial for mapping the magnetic field structure on the sky.

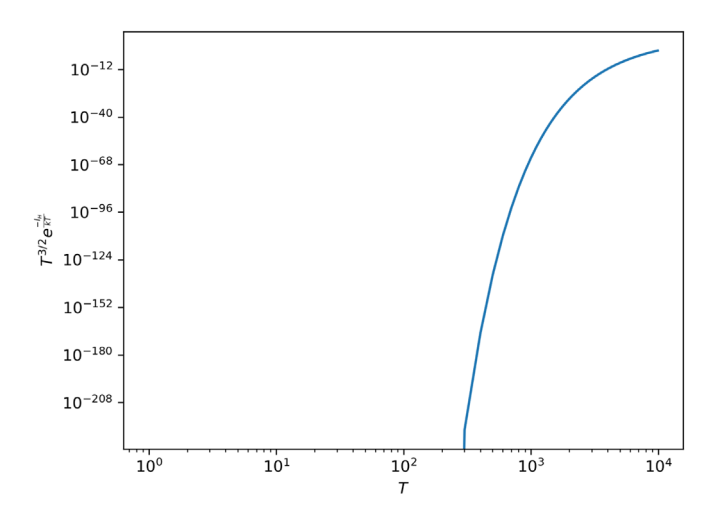


Figure 6. Change of the fraction function in Saha equilibrium with different temperatures under constant density.

6.2. Limitation of the Current Work

While we concisely compare the two magnetic field mapping techniques in this work, our work is limited to the isothermal environment. We aware that our study may not hold in the multi-phase environment, especially in cold gas. However, we believe our our results are relevant to more general situations including multi-phase media, and below we explain why. For instance, considering that multi-phase media are under Saha equilibrium locally, the thermal electron fraction is closely related to the temperature of the local environment, which is

$$\frac{X^2}{1-X} = \frac{1}{n_{\rm H}} \left(\frac{2\pi m_e kT}{h^2}\right)^{3/2} e^{-\frac{I_{\rm H}}{kT}}.$$
 (22)

When X is the fraction between ionized hydrogen and natural hydrogen, T is the temperature, n_h is the density of the hydrogen, I_H is the ionized energy of the hydrogen, m_e is the electron mass, k is Boltzmann's constant, and k is the Planck constant. By calculating the ionized hydrogen fraction, we can also determine the density of the thermal electron. Figure 6 shows the change of $T^{3/2}e^{-I_H/kT}$ in different T with the

Table 4
Summary of the Differences between the SPG and FT Methods

	Synchrotron Polarization Gradients	FT
2D/3D Structure	Yes	No
Order Info	Yes	Generally No
Dependence of the obtained magnetic field	As a function of line of sight distance	As a function of Faraday depth ϕ
Intensity profile along LOS	No	Yes
Data Point Requirement	Two frequency measurements are required	A vast number of measurements are required
Accuracy	Relatively Low	Depends on the frequency density and range

assumption of constant density. We see that the relation is dominated by the exponential term and drops rapidly when T is small (about 10^2 K). This result does not change much even though the cold gas may be 4–5 orders denser than the hot gas. Therefore, we expect the hot and warm phases to dominate over the emission of the the cold phases, as discussed in Lazarian & Pogosyan (2016) and references therein for external ionization sources.

In particular, Kritsuk et al. (2007) showed that the volume fraction of cold gas fills up a small fraction of the space (from 7% to 8%) in 512³ numerical simulations. Most of the space in the environment is suffused with warm and hot gas. This also indicates that the principal emission source in the multi-phase gas that we observed is coming from hot and warm gas. In addition, the fraction of cold gas decreases substantially for high latitudes (see Kalberla & Haud 2018).

We believe that synchrotron emissions are mainly aroused from hot and warm gas phases, which indicates the sonic Mach number is sufficiently low and the density variation is negligible. Moreover, the Faraday rotation term $RM \propto \int dz n_{th} B_z$ can be approximated with cumulative sum of magnetic field strength along the LOS. Therefore, the synchrotron emission $P \sim Pi \exp(iRM)$ is independent of density variation, and also the variation from the equation of state. A case in which an arbitrary equation of state and in which the media have fluctuations of density and magnetic field was performed analytically in Lazarian & Pogosyan (2016). Comparatively, our study shows that using isothermal simulations does not omit the essential physics. More complicated cases discussed in Lazarian & Pogosyan (2016) will be considered elsewhere.

7. Synergy of the Two Approaches

The multi-frequency measurements of synchrotron polarization allow a synergistic use of the two techniques. The physical processes of inversion upon which the two techniques are different. This allows greater insights. The SPG uses the depolarization of the signal to trace the magnetic field. Therefore, the SPG results do not depend on the variations of the magnetic field direction along the LOS. As a consequence, one can combine the SPG with the FT and use the SPG to resolve the FT problems illustrated in Figure 3, by placing the sources in the right sequence along the LOS. The FT can improve the accuracy of the detailed tracing of the magnetic field, provided that the frequency coverage is sufficiently high. We summarize the difference of key features between two methods in Table 4. Combining these approaches could be a fruitful direction for future research.

8. Summary

This paper compares the FT and SPGs techniques, which can both plausibly trace the 3D magnetic field using polarized synchrotron emission. We have explored numerically the performance of these techniques and analyzed their strengths and limitations in the special cases of uniform and isothermal turbulent media. The FT method can provide high-accuracy magnetic field tracing, provided there is wide frequency band coverage, high frequency resolution is available, and the mean magnetic field is not too close to being perpendicular to the LOS. It is advantageous that the SPGs, on the other hand, provide a better accuracy for tracing the 3D magnetic field when the magnetic field is nearly perpendicular to the LOS. Moreover, we demonstrated that the SPGs require less frequencies when restoring the magnetic field structure. As a result, we claim that combining the two techniques is advantageous, especially as the SPG technique matures and becomes more accurate.

A.L. acknowledges the support of NSF grants DMS 1622353, AST 1715754, and 1816234.

References

```
Armstrong, J. W., Rickett, B. J., & Spangler, S. R. 1995, ApJ, 443, 209
Brentjens, M. A., & de Bruyn, A. G. 2005, A&A, 441, 1217
Burkhart, B., Collins, D. C., & Lazarian, A. 2015, ApJ, 808, 48
Burn, B. J. 1966, M
                     RAS, 133, 67
Caldwell, A., Dvali, G., Majorovits, B., et al. 2017, PhRvL, 118, 091801
Chepurnov, A., & Lazarian, A. 2009, ApJ, 693, 1074
Chepurnov, A., & Lazarian, A. 2010, ApJ, 710, 853
Cho, J., Lazarian, A., & Vishniac, E. T. 2002, ApJL, 566, L49
Cho, J., & Vishniac, E. T. 2000, ApJ, 539, 273
Dickey, J. M., Landecker, T. L., Thomson, A. J. M., et al. 2019, ApJ, 871, 106
Draine, B. T. 2009, SSRv, 143, 333
Esquivel, A., & Lazarian, A. 2005, ApJ, 631, 320
Farnes, J. S., Heald, G., Junklewitz, H., et al. 2018, MNRAS, 474, 3280
Goldreich, P., & Sridhar, S. 1995, ApJ, 438, 763
González-Casanova, D. F., & Lazarian, A. 2017, ApJ, 835, 41
Haverkorn, M. 2018, in IAU Symp. 333, Peering towards Cosmic Dawn, ed.
   T. van der Hulst & V. Jelić (Cambridge: Cambridge Univ. Press), 129
Heyer, M., Gong, H., Ostriker, E., & Brunt, C. 2008, ApJ, 680, 420
Higdon, J. C. 1984, ApJ, 285, 109
Jelic, V., de Bruyn, A. G., Pandey, V. N., et al. 2015, A&A, 583, A137
Jelic, V., Prelogovic, D., et al. 2018, A&A, 615, L3
Jokipii, J. R. 1966, ApJ, 146, 480
Kalberla, P. M. W., & Haud, U. 2018, A&A, 619, A58
Kandel, D., Lazarian, A., & Pogosyan, D. 2017, MNRAS, 464, 3617
Kritsuk, A. G., Ustyugov, S. D., & Norman1, M. L. 2017, NJPh, 19, 065003
Lazarian, A. 2007, JOSRT, 106, 225
Lazarian, A., & Pogosyan, D. 2012, ApJ, 747, 5
Lazarian, A., & Pogosyan, D. 2016, ApJ, 818, 178
Lazarian, A., Pogosyan, D., & Esquivel, A. 2002, in ASP Conf. Proc. 276,
   Seeing Through the Dust: The Detection of HI and the Exploration of the
   ISM in Galaxies, ed. A. R. Taylor, T. L. Landecker, & A. G. Willis (San
```

Francisco, CA: ASP), 182

```
Lazarian, A., & Vishniac, E. T. 1999, ApJ, 517, 700
Lazarian, A., & Yuen, K. H. 2018a, ApJ, 853, 96
Lazarian, A., & Yuen, K. H. 2018b, ApJ, 865, 59
Li, F., Brown, S., Cornwell, T. J., & de Hoog, F. 2011, A&A, 531, A126
Mac Low, M.-M., & Klessen, R. S. 2004, RvMP, 76, 125
Maron, J., & Goldreich, P. 2001, ApJ, 554, 1175
McKee, C. F., & Ostriker, E. C. 2007, ARA&A, 45, 565
```

```
Robitaille, J.-F., Scaife, A. M. M., Carretti, E., et al. 2017, MNRAS, 468, 2957
Van Eck, C. L., Haverkorn, M., Alves, M. I. R., et al. 2017, A&A, 597, A98
Yan, H., & Lazarian, A. 2008, ApJ, 673, 942
Yuen, K. H., Chen, J., Hu, Y., et al. 2018, ApJ, 865, 54
Yuen, K. H., & Lazarian, A. 2017, ApJL, 837, L24
Zaldarriaga, M., & Seljak, U. 1997, PhRvD, 55, 1830
```